TECHNICAL REVIEW

NO. 1 – 2014

Experimental Characterization of Operating Bladed Rotor Using HPS and SSI Techniques

Microphone Acoustic Impedance in Reciprocity Calibration

Brüel & Kjær
BEYOND MEASURE

Previously issued numbers of Brüel & Kjær Technical Review

(Continued on cover page 3)

Technical Review

No. 1 – 2014

Contents

Editor: Harry K. Zaveri

Experimental Characterization of Operating Bladed Rotor Using Harmonic Power Spectra and Stochastic Subspace Identification[1]

D.Tcherniak[2], S. Yang[3], M.S. Allen[4]

Abstract

The dynamic response of mechanical systems with rotating elements, such as operating wind turbines, cannot be described using a classical linear time-invariant (LTI) formulation because the mass and stiffness matrices can vary periodically during rotation. Such systems belong to the class of linear periodic time-variant (LPTV) systems and require special treatment for their experimental identification. For instance, the Harmonic Power Spectra (HPS) method, which is based on Floquet theory, can be applied. Afterwards, the experimental responses are modulated exponentially using the rotational frequency. The HPS matrix is computed between the modulated responses and is used as the input for Operational Modal Analysis (OMA). OMA provides the frequencies of the modes and the Fourier coefficients for reconstructing the time-periodic mode shapes. In the authors' prior publications, the HPS method is applied to the frequency domain. This study extends the HPS method to the time domain and makes it possible to use powerful stochastic subspace identification (SSI) techniques for modal identification. This leads to more accurate parameter estimates and can be used on modes with close frequencies. The advantage of the suggested approach is that it allows for the use of existing implementations of SSI and thus provides a simple tool for modal identification of periodic systems.

---

1 First Published in ISMA Conference 2014

2 Brüel & Kjær Sound and Vibration Measurement
Skodsborgvej 307, Nærum 2850, Denmark

3 Turbomachinery Systems, Praxair Inc.
175 East Park Drive, Tonawanda, NY 14150

4 Department of Engineering Physics, University of Wisconsin-Madison
535 Engineering Research Building, 1500 Eng. Drive, Madison, WI 53706, USA

Résumé

La réponse dynamique des systèmes mécaniques intégrant des éléments tournants, par exemple des éoliennes, ne peut faire l'objet d'une formulation LTI (linear time-invariant) puisque les matrices de masse et de rigidité peuvent varier périodiquement pendant la rotation. Ces systèmes, dits sytèmes LPTV (linear periodic time-variant) nécessitent un traitement particulier pour pouvoir être identifiés expérimentalement. C'est une méthode faisant intervenir les spectres de puissance harmoniques (méthode HPS basée sur la théorie de Floquet) qui est ici appliquée. Ensuite, les réponses sont modulées exponentiellement en utilisant la fréquence de rotation. La matrice HPS est calculée entre les réponses modulées puis utilisée comme donnée d'entrée pour une analyse modale en fonctionnement (analyse OMA). Cette analyse fournit les fréquences des différents modes et les coefficients de Fourier pour reconstruire les déformées modales variant périodiquement dans le temps. Dans les publications précédentes de l'auteur, la méthode HPS était appliquée au seul domaine fréquentiel. La présente étude étend la méthode HPS au domaine temporel, rendant possible l'utilisation de puissantes techniques SSI (stochastic subspace identification) pour l'identification modale. Cela conduit à des estimations plus précises des paramètres et peut être utilisé pour les modes caractérisés par des fréquences proches. L'avantage de l'approche ici suggérée est qu'elle permet d'utiliser des applications existantes de la technique SSI et qu'elle constitue donc un outil simple pour l'identification des modes des systèmes périodiques.

Zusammenfassung

Das dynamische Verhalten mechanischer Systeme mit rotierenden Elementen, beispielsweise beim Betrieb von Windturbinen, lässt sich nicht mit einer klassischen linearen zeitinvarianten (LTI) Formel beschreiben, weil die Masse- und Steifigkeits-Matrix während der Rotation periodisch variieren kann. Diese Systeme gehören zur Klasse der periodisch zeitvarianten linearen (LPTV) Systeme und erfordern eine besondere Behandlung, um experimentell identifiziert werden zu können. Beispielsweise kann die Methode der Harmonic Power Spectra (HPS) verwendet werden, die auf der Floquet-Theorie beruht. Anschließend werden die experimentell erhaltenen Antwortfunktionen mit Hilfe der Rotationsfrequenz exponentiell moduliert. Die HPS-Matrix wird zwischen den modulierten Antwortfunktionen berechnet und als Eingabe für die Operational Modal Analysis (OMA) verwendet. OMA liefert die Frequenzen der Moden sowie die Fourier-Koeffizienten zur Rekonstruktion der zeitlich periodischen

Modenformen. In den früheren Veröffentlichungen der Autoren wurde die HPS-Methode auf den Frequenzbereich angewendet. Mit dieser Studie wird die HPS-Methode auf den Zeitbereich erweitert, wodurch leistungsfähige Techniken der Stochastic Subspace Identification (SSI) zur Modenidentifikation verwendet werden können. Dies führt zu präziseren Parameterbestimmungen und ist für Moden mit eng benachbarten Frequenzen geeignet. Der Vorteil des empfohlenen Verfahrens besteht darin, dass es die Nutzung bestehender SSI-Implementierungen ermöglicht und somit ein einfaches Werkzeug für die Modenidentifikation von periodischen Systemen bereitstellt.

1. Introduction

Operational modal analysis (OMA) [1], a method of extracting the modes and hence a linear dynamic model of a structure from operational measurements, has become a mainstream technology in the past few decades. Often the structures of interest involve rotating machinery such as operating wind turbines. This makes the application of well established OMA techniques invalid since the structure under test is not time-invariant and, therefore, violates the main assumption of modal analysis. If the structural properties change periodically, the structure can be modelled as a linear periodic time-variant (LPTV) system. Currently, the number of studies on identification of LPTV systems is limited. Study [2] suggests using the Coleman, or multiblade coordinate (MBC), transformation as a preprocessing step to OMA. By changing the variables to a rotational frame, the Coleman transformation converts the LPTV system to LTI. This allows for the application of a wide range of classical modal identification techniques. However, this method can only be applied to isotropic rotors, meaning all blades have identical mass and structural properties. In additon, for rotors rotating in a verticle plane, as in the case of horizontal axis wind turbines (HAWT), gravity introduces forces that break symmetry and can cause the system to exhibit linear time-periodic behaviour. This prevents the use of the Coleman transformation for in-plane modes. Jhinaoui [3] suggests a subspace identification method that is specially developed for rotating systems. The method identifies the underlying Floquet eigenstructure of the rotating system and uses samples taken at the same position of the rotor in consecutive revolutions. Allen suggests using harmonic power spectra (HPS) for structure identification then extends experimental modal analysis to LPTV systems [4] and, later, to OMA [5]. This framework has been used quite extensively to extract the mode shapes from continuous-scan laser vibrometer measurements [6-9], and the authors recently applied it to measurements from an operating wind turbine [10].

The first step when computing HPS is to modulate the measured time histories by multiplying them by $e^{-\mathrm{i}m\Omega t}$, where Ω is the rotational frequency of the turbine and m is some integer. Then, the theory shows that the augmented set of measurements can be processed using standard curve-fitting techniques or peak picking to extract the natural frequencies and damping ratios. The theory also explains how to relate the amplitudes of the harmonics in response to the time-varying mode shapes. The method described in [5] uses *frequency-domain* modal algorithms to extract modal parameters. In this paper, the method is referred to as H-OMA-FD and is extended to the *time domain* OMA; the suggested approach is referred to as H-OMA-TD.

The consequence of the harmonic modulation process is that it makes the modulated time series complex and, hence, is not amenable to analysis by conventional OMA/SSI routines. This article proposes an approach that circumvents this difficulty so that powerful and robust OMA/SSI algorithms can be used to extract the structure's modal parameters.

2. Theoretical Background

The state space model of a linear time-periodic system with N degrees of freedom can be written as

$$\begin{aligned} \dot{\mathbf{x}}(t) &= \mathbf{A}(t)\mathbf{x}(t) + \mathbf{B}(t)\mathbf{u}(t) \\ \mathbf{y}(t) &= \mathbf{C}(t)\mathbf{x}(t) + \mathbf{D}(t)\mathbf{u}(t) \end{aligned} \tag{1}$$

where $\mathbf{A}(t)$ is the system matrix, $\mathbf{B}(t)$ is the input matrix, $\mathbf{C}(t)$ is the output matrix and $\mathbf{D}(t)$ is the direct input matrix, and all are periodic with time. For example, the classical system with mass, damping and stiffness matrices $\mathbf{M}$, $\mathbf{C}_d$ and $\mathbf{K}$ with the equation of motion

$$\mathbf{M}(t)\ddot{\mathbf{z}}(t) + \mathbf{C}_d(t)\dot{\mathbf{z}}(t) + \mathbf{K}(t)\ddot{\mathbf{z}}(t) = \mathbf{f}(t) \tag{2}$$

can be written in this form using $\mathbf{x}(t) = [\mathbf{z}(t)^T \ \ \dot{\mathbf{z}}(t)^T]^T$ [6]. For any initial state and input pair $(\mathbf{x}(t_0), \mathbf{u}(t_0))$, a unique solution $\mathbf{y}(t)$ exists and can be written in terms of the state transition matrix $\mathbf{\Phi}(t, t_0)$ [12].

$$\mathrm{y}(t) = \mathbf{C}(t)\mathbf{\Phi}(t, t_0)\mathbf{x}(t_0) + \mathbf{C}(t)\int_{t_0}^{t}\mathbf{\Phi}(t, \tau)\mathbf{B}(\tau)\mathbf{u}(\tau)d\tau + \mathbf{D}(t)\mathbf{u}(t) \tag{3}$$

The general solution (with the direct input matrix $\mathbf{D}(t)$ equal to zero) is the basis for Floquet analysis and is used to derive the harmonic transfer function and HPS used in operational modal analysis [5, 13].

2.1 Floquet Analysis

The state transition matrix $\mathbf{\Phi}(t, t_0)$ is the key to obtaining the general solution in Eq. (3). When the system is linear time-invariant, or $\mathbf{A}(t) = \mathbf{A}$, and the other coefficient matrices are constant, the state transition matrix is $e^{\mathbf{A} \times (t,\, t_0)}$ and can be further decomposed as

$$\mathbf{\Phi}(t, t_0) = e^{\mathbf{A} \times (t - t_0)} = \mathbf{P}e^{\mathbf{\Lambda} \times (t - t_0)}\mathbf{P}^{-1} \tag{4}$$

where $\mathbf{P}$ is the matrix of eigenvectors of the system matrix $\mathbf{A}$, and $\mathbf{\Lambda}$ is a diagonal matrix of eigenvalues.

On the other hand, when the system is periodic and satisfies the condition $\mathbf{A}(t) = \mathbf{A}(t + \mathrm{T})$ where $\mathrm{T} = 2\pi/\Omega$ is the fundamental period, the dynamics of the periodic system have to be studied using Floquet theory [12, 14-16] because $\mathbf{\Phi}(t, t_0) \neq e^{\mathbf{A}(t) \times (t,\, t_0)}$. The Floquet theory introduces a coordinate change to the system matrix $\mathbf{A}(t)$ and transforms the LPTV system to an LTI system. As a result, the state transition matrix becomes

$$\mathbf{\Phi}(t, t_0) = \bar{\mathbf{P}}(t)e^{\mathbf{L} \times (t - t_0)}\bar{\mathbf{P}}(t_0)^{-1} \tag{5}$$

where $\bar{\mathbf{P}}(t)$ is a periodic matrix. The eigenvalues of $\mathbf{L}$ are called *Floquet exponents* [15,16], and it is important to note that they are constant even though $\mathbf{A}(t)$ is time-periodic. If all Floquet exponents are non-zero and non-repeated, that is, $\mathbf{L}$ is nonsingular, then there exists a nonsingular matrix $\mathbf{R}$ that diagonalizes $\mathbf{L}$ with $\mathbf{L} = \mathbf{R\Lambda R}^{-1}$. Then, the state transition matrix in Eq. (5) becomes

$$\mathbf{\Phi}(t, t_0) = \mathbf{P}(t)e^{\mathbf{\Lambda} \times (t - t_0)}\mathbf{P}(t_0)^{-1} \tag{6}$$

where $\mathbf{P}(\mathrm{t}) = \bar{\mathbf{P}}(t)\mathbf{R}$ is a matrix of time-periodic eigenvectors for the LPTV system [17]. The state transition matrix is decomposed into the modal summation form

$$\mathbf{\Phi}(t, t_0) = \sum_{r=1}^{2N} \boldsymbol{\psi}_r(t)\boldsymbol{L}_r(t_0)e^{\lambda_r(t - t_0)} \tag{7}$$

where $\boldsymbol{\psi}_r(t)$ is the r^{th} column of $\mathbf{P}(t)$, and $\mathbf{L}_r(t)$ is the r^{th} row of $\mathbf{P}(t)^{-1}$. λ_r is the r^{th} Floquet exponent that is analogous to the r^{th} eigenvalue of an LTI system. The r^{th} Floquet exponent can be written in terms of the damping ratio ζ_r and natural frequency ω_r as $\lambda_r = -\zeta_r\omega_r + \mathrm{i}\omega_r\sqrt{1-\zeta_r^2}$ for an underdamped mode. Thus, the steady state response $\mathbf{y}(t)$ in Eq. (3) becomes

$$\begin{aligned} \mathbf{y}(t) &= \sum_{r=1}^{n} \mathbf{R}_{y,r}(t)e^{\lambda_r(t - t_0)} \\ \mathbf{R}_{y,r}(t) &= \mathbf{C}(t)\boldsymbol{\psi}_r(t)\mathbf{L}_r(t_0)\mathbf{x}(t_0) \end{aligned} \tag{8}$$

The residue matrix $\mathbf{R}_{y,r}(t)$ is periodic and can be expanded into a Fourier series. Assume that the residue matrix can be adequately represented using a fixed number, $2N_B + 1$, of terms

$$\mathbf{R}_{y,r}(t) = \sum_{n=-N_B}^{N_B} \mathbf{B}_{n,r}\, e^{\mathrm{i}n\Omega(t - t_0)} \tag{9}$$

where $\mathbf{B}_{n,r}$ is the n^{th} Fourier coefficient matrix of the r^{th} mode. So, the output $\mathbf{y}(t)$ becomes

$$\mathbf{y}(t) = \sum_{r=1}^{2N} \sum_{n=-N_B}^{N_B} \mathbf{B}_{n,r} e^{(\lambda_r + \mathrm{i}n\Omega)(t - t_0)} . \tag{10}$$

This equation reveals that the response of each mode in the system is a sum of damped sinusoids with several sideband harmonics around each natural frequency.

2.2 Harmonic Transfer Function

Similar to what is shown above for the transient response, when an LPTV system is excited by a sinusoidal force at some frequency, the response will be at the same frequency and at an infinite number of its harmonics, each separated by the fundamental frequency Ω. At first glance, it seems that it is impossible to use a linear transfer function for such a system. However, Wereley overcomes this difficulty by augmenting the input and output signals with frequency shifted copies of each. Then the couplings between the frequencies can be accounted for in the augmented version [18]. Specifically, the m^{th} modulated signal is given by

$$\mathbf{y}_m(t) = \mathbf{y}(t)e^{-\mathrm{i}m\Omega t} \tag{11}$$

for $m \in \mathbb{N}$, where $m = -M \ldots M$. The Fourier transformation of each signal is denoted as $\mathbf{y}_m(\omega)$. $\mathbf{Y}(\omega) = [\ldots \mathbf{y}_{-1}^T(\omega) \;\; \mathbf{y}_0^T(\omega) \;\; \mathbf{y}_1^T(\omega) \ldots]^T$ is the collection of frequency shifted copies, and the harmonic transfer function (HTF) can be established for the LPTV system. The HTF is completely analogous to the commonly known transfer function for LTI systems.

The HTF is derived by inserting the modulated signal from (11) into the general solution in Eq. (3), and using the modal solution from Eq. (7). The harmonic balance approach is used to match the terms with the same frequency in the exponent $e^{(\mathrm{i}\omega + \mathrm{i}m\Omega)t}$. After much algebra and organization, a harmonic transfer function

$$\mathbf{Y}(\omega) = \mathbf{G}(\omega)\mathbf{U}(\omega) \tag{12}$$

is obtained in terms of the modal parameters of the state transition matrix, where $\mathbf{U}(\omega) = [\ldots \mathbf{u}_{-1}^T(\omega) \;\; \mathbf{u}_0^T(\omega) \;\; \mathbf{u}_1^T(\omega) \ldots]^T$ is the exponentially modulated input in the frequency domain and

$$\begin{aligned} \mathbf{G}(\omega) &= \sum_{r=1}^{2N} \sum_{l=-\infty}^{\infty} \frac{\bar{\mathbf{c}}_{r,l}\bar{\mathbf{b}}_{r,l}}{\mathrm{i}\omega - (\lambda_r - \mathrm{i}l\omega_A)} \\ \bar{\mathbf{c}}_{r,l} &= [\ldots \quad \bar{c}_{r,-1-l} \quad \bar{c}_{r,-l} \quad \bar{c}_{r,1-l} \quad \ldots]^T \\ \bar{\mathbf{b}}_{r,l} &= [\ldots \quad \bar{b}_{r,l+1} \quad \bar{b}_{r,l} \quad \bar{b}_{r,l-1} \quad \ldots]. \end{aligned} \tag{13}$$

The m^{th} term in the vector $\bar{\mathbf{c}}_{r,l}$ is $\bar{c}_{r,l}$, which is the $(m-1)^{\text{th}}$ Fourier coefficient (or vector of Fourier coefficients) of $\mathbf{C}(t)\boldsymbol{\psi}_r(t)$. Note that the mode vectors $\bar{\mathbf{c}}_{r,l}$ acquired at different peaks describe the same shape, but the elements are shifted in position for each vector. For example, suppose that the mode vector at frequency λ_r is $\bar{\mathbf{c}}_{r,0} = [0 \;\; a \;\; b \;\; c \;\; 0]^{\mathrm{T}}$. Then the mode vector at $\lambda_r + \Omega$ should be

$\bar{\mathbf{c}}_{r,-1} = [\mathrm{a\ \ b\ \ c\ \ 0\ \ 0}]^{\mathrm{T}}$ multiplied by an unknown constant, and the mode vector at $\lambda_r - \Omega$ should be proportional to $\bar{\mathbf{c}}_{r,1} = [\mathrm{0\ \ 0\ \ a\ \ b\ \ c}]^{\mathrm{T}}$. A least squares approach can be used to extract the best estimate of the mode vector $\bar{\mathbf{c}}_{r,l}$ from the multiple estimations. Similarly, $\bar{\mathbf{b}}_{r,l-m}$ is the $(l-m)^{\mathrm{th}}$ Fourier coefficient of $\mathbf{L}_r(t)^{\mathrm{T}}\mathbf{B}(t)$.

2.3 Harmonic Power Spectrum

In practice, there exists a measured response of an LPTV system to an excitation that satisfies OMA assumptions where the measured responses are a collection of time histories recorded at N_0 DOFs with $\mathbf{y}(t) \in \mathbb{R}^{N_0}$ and sampled with sampling frequency F_S. These time histories are then exponentially modulated by multiplying by $e^{-\mathrm{i}m\Omega t}$, where $m = -M \ldots M$, to obtain a collection of responses $\mathbf{y}_m(t) \in \mathbb{C}^{N_0(2M+1)}$. Then the harmonic power spectrum (HPS) matrix can be found in the conventional manner, as in the LTI case:

$$\mathbf{S}_{YY}(\omega) = \mathrm{E}(\mathbf{y}_m(\omega)\mathbf{y}_m(\omega)^{\mathrm{H}}) \tag{14}$$

where E() is the expectation, and $()^{\mathrm{H}}$ denotes the Hermitian transpose. Retaining only the dominant terms, the HPS can be written in terms of the modes of the LPTV system as

$$\mathbf{S}_{YY}(\omega) \approx \sum_{r=1}^{2N} \sum_{l=-\infty}^{\infty} \frac{\bar{\mathbf{c}}_{r,l}\mathbf{W}(\omega)_r \mathbf{c}_{r,l}^{\mathrm{H}}}{[\mathrm{i}\omega - (\lambda_r - \mathrm{i}l\Omega)][\mathrm{i}\omega - (\lambda_r - \mathrm{i}l\Omega)]^{\mathrm{H}}} . \tag{15}$$

The terms $(\lambda_r - \mathrm{i}l\Omega)$ cause the HPS to have a peak near the system's eigenvalues (or Floquet exponents) λ_r and also at each eigenvalue plus some integer multiple of the fundamental frequency l. Here, $\mathbf{W}(\omega)_r$ is related to the autospectrum of the modulated input signal. In output-only modal analysis of LTI systems, the input is assumed to be uncorrelated, random white noise, and the autospectrum of the input signal becomes constant. The same assumption is used for LPTV systems.

The HPS has the same modal summation form as the power spectrum of an LTI system, which is

$$\mathbf{S}_{YY}^{LTI}(\omega) = \sum_{r=1}^{N} \frac{\varphi_r S_{UU}^{LTI}(\omega)\varphi_r^{\mathrm{H}}}{[\mathrm{i}\omega - \lambda_r][\mathrm{i}\omega - \lambda_r]^{\mathrm{H}}} . \tag{16}$$

This function produces a peak in the spectrum when the excitation frequency ω is near the natural frequency $\mathrm{Im}(\lambda_r)$, and the peak can be curve-fitted to identify the natural frequencies, damping ratios and mode shapes of the system. Hence, the same algorithms for LTI systems can be used to identify modal parameters of LPTV systems, and the same intuition that is used to interpret frequency response functions can also be used to interpret harmonic transfer functions. However, there are a few differences that must be noted in signal processing:

- Theoretically, an LPTV system has an infinite number of peaks for each mode. The peaks occur at the frequencies $\omega = \mathrm{Im}(\lambda_r - \mathrm{i}l\Omega)$. If the observed mode shapes $\mathbf{C}(t)\boldsymbol{\psi}_r(t)$ are constant in time, $\bar{\mathbf{c}}_{r,l}$ and $\bar{\mathbf{b}}_{r,l}$ each contain only one nonzero term: $\bar{c}_{r,0}$ and $\bar{b}_{r,0}$. Then, Eq. (13) and (15) reduce to the familiar relationship for an LTI system.
- The mode vectors of an LTI system describe the spatial pattern of deformation of a mode. For an LPTV system, the vectors $\bar{\mathbf{c}}_{r,l}$ consist of the Fourier coefficients that describe the time-periodic spatial deformation pattern.

2.4 Complex Time Series: Rigorous Approach

In the approach outlined above, the measured signal $\mathbf{y}(t)$ is multiplied by $e^{-\mathrm{i}m\Omega t}$. Since $e^{-\mathrm{i}m\Omega t} = \cos(m\Omega t) - \mathrm{i}\sin(m\Omega t)$, it is possible to obtain the same result by multiplying the signals by sine and cosine to form the real and imaginary parts separately. Eq. (15) shows that the HPS is simply a sum of damped exponential terms. It can be shown that each term leads to an exponential term in the time domain and that they are of the form $\mathbf{A}_{r,l}e^{(\lambda_r - \mathrm{i}l\Omega)t}$.

The residue matrix at the l^{th} harmonic of the r^{th} mode is defined as

$$\mathbf{A}_{r,l} = \frac{\bar{\mathbf{c}}_{r,l}\mathbf{W}(\omega)_r\bar{\mathbf{c}}^{\mathrm{H}}_{r,l}}{\zeta_r\omega_r} . \tag{17}$$

Hence, if the signal is modulated using sine and cosine rather than $e^{-\mathrm{i}m\Omega t}$, and the residues obtained are $\mathbf{A}^{\mathrm{S}}_{r,l}$ and $\mathbf{A}^{\mathrm{C}}_{r,l}$ for the sine and cosine cases respectively, then the desired residues should simply be

$$\mathbf{A}_{r,l} = \mathbf{A}^{\mathrm{C}}_{r,l} - \mathrm{i}\mathbf{A}^{\mathrm{S}}_{r,l} . \tag{18}$$

The disadvantage of this approach is that the signals become twice as large (twice as many outputs) as compared to the case where complex time series are allowed.

Also, note that the sine and cosine terms should be treated simultaneously in a global curve-fitting algorithm to assure that the residues obtained correspond to precisely the same poles.

2.5 Simplified Approach

This algorithm takes a different approach, seeking to produce a time series that is real and yet has the same spectrum for all positive frequencies. To help explain it, first recall that when using the conventional approach, the HPS matrix $\mathbf{S}_{YY}(\omega)$ is formed as Eq. (14) and $\mathbf{S}_{YY}(\omega) \in \mathbb{C}^{N_0(2M+1)\times N_0(2M+1)}$. Then several rows of the matrix are selected, and peak-picking is used to determine the modal parameters. It is important to note that for peak-picking, only the frequencies in the range $0 < \omega < \pi F_S - M\Omega$, or the positive part of the frequency axis, are used.

This study suggests replacing the frequency domain peak-picking method by more robust OMA/SSI algorithms, which are available in some commercial software packages (for example, Brüel & Kjær Type 7780). Thus, the combination of SSI with exponential modulation will allow for traditional OMA/SSI algorithms to be readily applied to LPTV systems.

However, the problem is that the commercial OMA/SSI does not accept complex time histories. To circumvent this limitation, assume there is a procedure that converts the exponentially modulated time histories $\mathbf{y}_m(t) \in \mathbb{C}$ to new time histories $\tilde{\mathbf{y}}_m(t)$ with the following properties:

$$\tilde{\mathbf{y}}_m^{(n)}(t) \in \mathbb{R} \text{ and} \tag{19}$$

$$\mathcal{F}(\tilde{\mathbf{y}}_m(t)) = \mathcal{F}(\mathbf{y}_m(t)) \text{ for } \omega \in [0, \pi F_S] \tag{20}$$

where $\mathcal{F}$ denotes the Fourier transform. The first property ensures the new signals are usable in the available implementations of the OMA/SSI algorithms, while the second means that

$$\tilde{\mathbf{S}}_{YY}(\omega) = \mathbf{S}_{YY}(\omega) \text{ for } \omega \in [0, \pi F_S]. \tag{21}$$

In other words, the new time histories $\tilde{\mathbf{y}}_m(t)$ have the same frequency content and phase relationships as the positive half of the harmonic power spectra utilized in the HPS method.

From Eq. (19) and (20), one can readily derive the algorithm converting $\mathbf{y}_m(t)$ to $\tilde{\mathbf{y}}_m(t)$ as follows:

1) Given exponentially modulated signals $\mathbf{y}_m(t)$, compute their periodogram $\mathcal{F}(\mathbf{y}_m(t))$ using a fast Fourier transform. The periodogram of complex $\mathbf{y}_m(t)$ is not a Hermitian function so its negative frequency component is not a complex conjugate of the positive frequency component.
2) Replace the negative frequency component of the periodogram with the complex conjugate of the positive component.
3) Using inverse FFT, generate new time signals $\tilde{\mathbf{y}}_m(t)$ that satisfy Eq. (19) and (20).

3. Results

To demonstrate the algorithm, consider a simple three-bladed rotor system which is a rough model of a horizontal axis wind turbine (Fig. 1). Each blade is modelled as a two-beam assembly; the beams are connected by a hinge with a linear angular spring of stiffness k_j, where $j = 1, 2, 3$ is the blade index. A lumped mass m_j is attached to the end of the outer beam. The azimuth angles of the blades are $\psi_j = \Omega t + 2\pi(j - 1)/3$, where the rotor angular speed Ω is assumed constant. The rotor is attached to the nacelle C with mass m_N. It is supported by the 'tower' and is modelled by two springs with stiffnesses k_H and k_V. The rotor is linked to the 'drivetrain' with moment of inertia I_D and stiffness k_D.

Fig. 1. Three-bladed rotor system

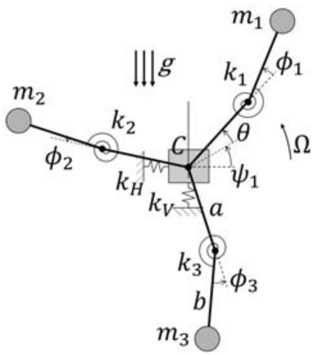

For examination of the rotor modal behaviour, the following parameters are chosen (same as in [18]):

- $a = b = 13.1$ m
- $k_1 = k_2 = k_3 = 2.006 \times 10^8$ N · m
- $m_1 = m_2 = m_3 = 41.7 \times 10^3$ kg
- $\Omega = 2\pi\ 0.16$ rad/s
- $m_N = 446 \times 10^3$ kg
- $k_H = 2.6 \times 10^6$ N/m
- $k_V = 5.2 \times 10^8$ N/m
- $I_D = 2.6 \times 10^7$ kg · m^2
- $k_D = 10^8$ N · m

These parameters approximate a generic 10 MW wind turbine model.

The identical system is considered in [18], where the equations of motion are set up and Floquet analysis is applied to investigate the influence of the rotor's anisotropy on the whirling components of the mode shapes.

Since this system has six degrees of freedom, six modes are expected and are named as follows:

- the *vertical* and *horizontal* modes, dominated by vertical and horizontal motion of the mass *C*
- three rotor modes: one symmetric (also called *collective*), where all blades deflect in-phase, and two anti-symmetric, also called *whirling*
- a '*drivetrain*' mode, where most of the potential energy is stored in the stiffness k_D.

One should not expect pure modes as there is always some degree of interaction; the names are only given to reflect the dominating motion of the mode. This study focuses on the rotor modes since they have the most pronounced periodic behaviour.

In the following, three methods are applied to the system. First, it is assumed that the equations of motion are known so Floquet analysis can be applied to generate an (almost) exact solution. This solution serves as the baseline for comparison with the other two methods. Next, an experimental scenario is simulated. It is assumed that the equations of motion are unknown, but it is possible to observe the response of the system to excitation. This satisfies OMA assumptions that all DOFs are excited by uncorrelated broadband noise with a flat spectrum. Last, both the conventional frequency domain HPS method and the suggested time-domain method are applied to the observed response, and the results are compared.

3.1 Floquet Analysis

Floquet analysis (see [19] for an overview and detailed description) is applied to the system in Fig. 1 as described in [18]. As mentioned in the theoretical background, Floquet analysis provides a modal decomposition, but for an LPTV system, the modes are periodic. Following the conventional approach, each periodic mode is Fourier expanded to the harmonic (Fourier) components. The LTI system can then be thought of as a special case of LPTV, where each mode has only one non-zero Fourier component. It can be shown that, for an isotropic three-bladed rotor in the absence of gravity, each mode has three non-zero Fourier components. The Coleman transformation [20] utilizes this phenomena and allows for the conversion of the LPTV system to an LTI system. A stronger periodicity of the system matrix in Eq. (1) requires more Fourier components to be included for consideration. For rotors that are almost isotopic, only a few Fourier components have significant magnitude, and the smaller components can be neglected.

Fig. 2 (a) and (c) show the magnitudes of the harmonic components obtained via Floquet analysis for an isotropic rotor in the absence of gravity. Two modes are shown: forward whirling (FW) mode, which is dominated by x_C but named after its significant whirling component, and collective mode. The backward whirling (BW) mode is explained in detail in Fig. 3. As mentioned before, the modes of a three-bladed isotropic rotor in the absence of gravity can be fully described with only three Fourier components.

Fig. 2. Simulated experiment for an isotropic rotor in the abscence of gravity. ***a***,***b****: FW mode;* ***c***,***d****: collective mode;* ***a***,***c****: Floquet analysis results;* ***b***, ***d****: H-OMA-TD results*

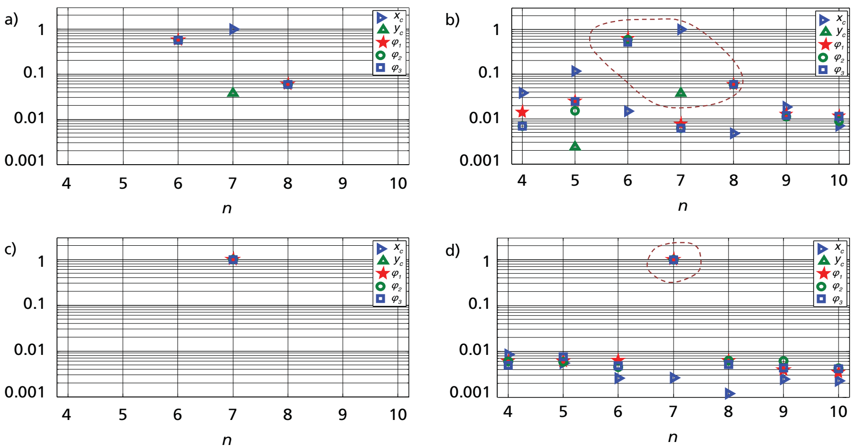

Fig. 3 focuses on the BW mode. Fig. 3 (b) shows the magnitude of its three non-zero Fourier components: FW component (A), motion of the center mass (B) and BW component (C). The BW component is about one order of magnitude higher than the FW component. It dominates the rotor dynamics, and the mode is named after this component. Fig. 3 (a) is a complexity plot that shows the phase relation between the three blades. The left plot is for the FW component (A), where the phase between the consecutive blades is +120°. The right plot is for the dominating BW component (C) with –120° phase.

Fig. 3. BW mode of an isotropic rotor with no gravity. ***a****: Shapes of the FW (left) and BW (right) components via Floquet analysis;* ***b****: Magnitude of the Fourier components via Floquet analysis;* ***c****: Shapes of the FW (left) and BW (right) via H-OMA- TD;* ***d, e, f****: Magnitudes of Fourier components for:* ***d****: n = –1,* ***e****: n = 0,* ***f****: n = +1, as in Table 1. The percent values in the boxes are a half-width of the pointwise 95% confidence bands computed based on five analysis, using Student's t-distribution*

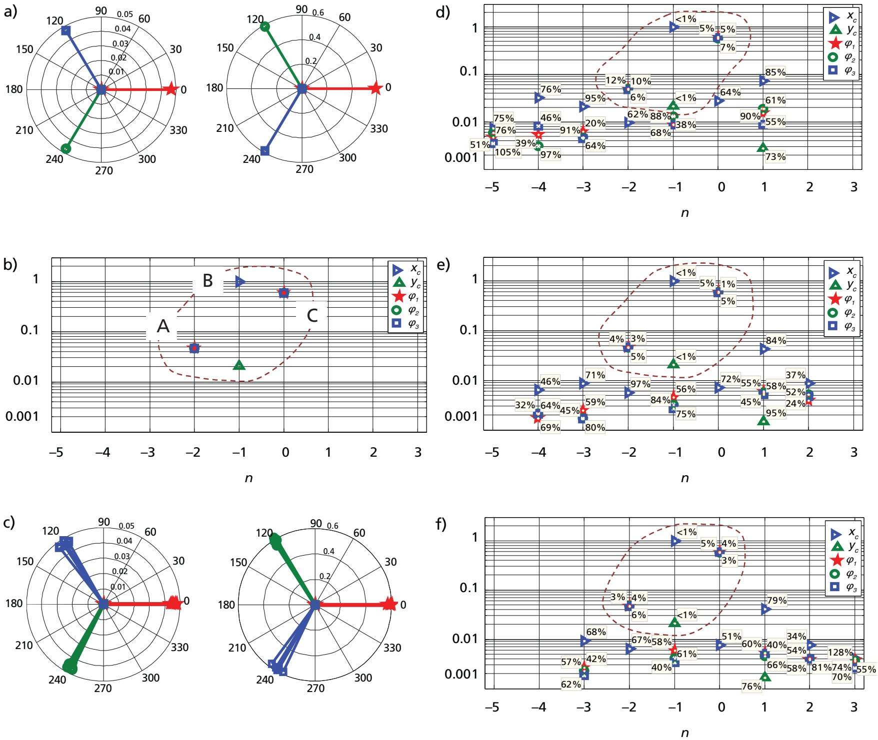

Fig. 4 (a), (c) and (f) show the BW, FW and collective modes for anisotropic rotor in the presence of gravity. Compared to the isotropic rotor, the system matrix of the anisotropic rotor demonstrates higher and more complex variation with time. As a result, it requires more Fourier components to describe the periodic mode shapes (compare with Fig. 2a, Fig. 2c and Fig. 3b).

*Fig. 4. Magnitudes of the Fourier components for anisotropic rotor: BW (top row), FW (middle row) and collective (bottom). **Left column**: results of the Floquet analysis; **right column**: H-OMA-TD for simulated experiment. Dashed lines show the significant components, dotted line shows the erroneous results due to vicinity to strong rotor harmonics*

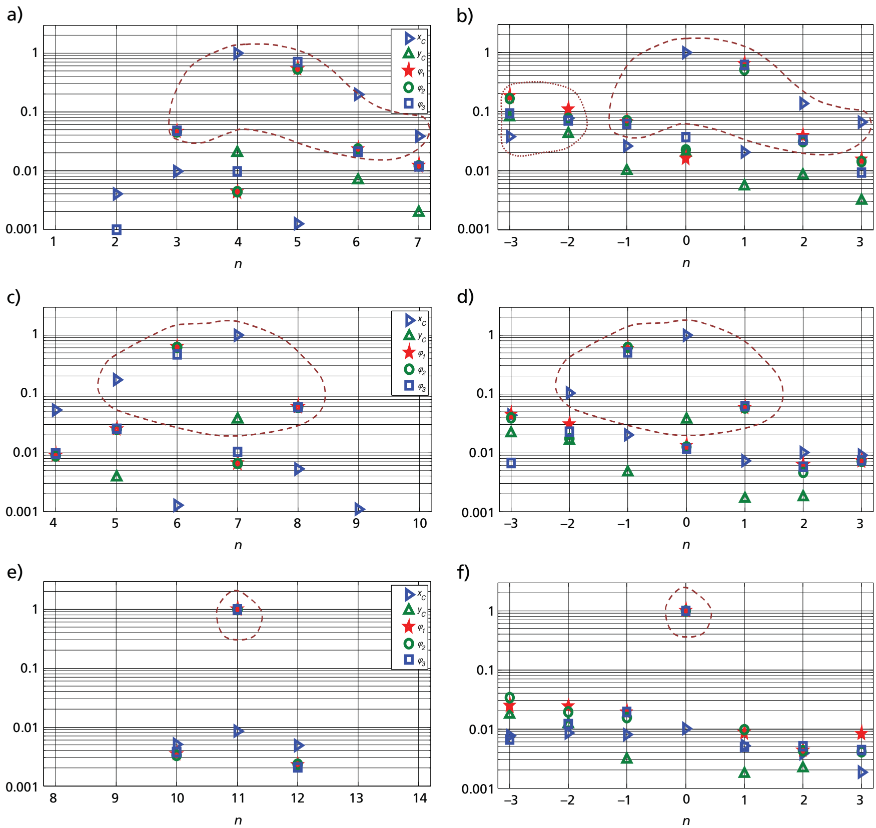

Table 1 provides the values of the Floquet exponents for both isotropic and anisotropic rotors.

Table 1. Floquet exponents obtained analytically, by H-OMA-TD and H-OMA-FD.

Mode Name	**Floquet exponent** $\lambda/(2\pi)$	n	**Un-aliased Floquet exponent** $(\lambda + n\Omega)/(2\pi)$	**H-OMA-TD (*n* = 0) (in Hz)**	**H-OMA-FD (in Hz)**
Isotropic rotor, no gravity					
BW	−0.0112 + 0.0764i	4	−0.0112 + 0.7164i	−0.0116(±0.0013) + 0.7162(±0.0008)i	−0.0140 + 0.7159i
FW	−0.0117 – 0.0610i	7	−0.0117 − 1.0590i	−0.0113(±0.0007) + 1.0587(±0.0025)i	−0.0102 + 1.0540i
Collective	−0.0348 + 0.0464i	11	−0.0348 + 1.8064i	−0.0353(±0.0014) + 1.8064(±0.0032)i	−0.0360 + 1.8006i
Anisotropic rotor, with gravity					
BW	−0.0111 + 0.0716i	4	−0.0111 + 0.7116i	−0.0122(±0.0018) + 0.7121(±0.0006)i	−0.0118 + 0.7129i
FW	−0.0116 − 0.0648i	7	−0.0116 − 1.0552i	−0.0113(±0.0008) + 1.0547(±0.0011)i	−0.0105 + 1.0549i
Collective	−0.0345 + 0.0378i	11	−0.0345 + 1.7985i	−0.0353(±0.0019) + 1.7985(±0.0032)i	−0.0286 + 1.7858i

3.2 Numerical Experiment

As input for the numerical experiment, the response of the rotor to uncorrelated broadband excitation is simulated. This excitation satisfies OMA assumptions, but it is acknowledged that the aeroelastic forces acting on the wind turbine rotor are, in reality, different [21]. The equations of motion are numerically integrated using fourth order Runge-Kutta method, for 7200 s (which corresponds to 1152 rotor revolutions).

3.2.1 Results from H-OMA-FD

The simulated turbine rotates at 0.16 Hz. The responses in the edgewise direction of all three blades ($\phi 1$, $\phi 2$, $\phi 3$) as well as the responses of the nacelle in the lateral (X_c) and vertical (Y_c) directions are collected into a response vector with 5 outputs. The responses are then exponentially modulated according to Eq. (11) with $m = -3 \ldots 3$. Then the modulated signals are split into 575 sub-blocks with a block size of 119 s (19 revolutions) with an 85% overlap. A Hanning window is applied to each block to reduce the leakage. The cross power spectra between the modulated signals and the original signals ($\phi 1$, $\phi 2$, $\phi 3$) are computed respectively in each sub-block and averaged over the whole time history. The resulting HPS matrix has 35 outputs (5 outputs with 7 harmonics for each output) by 3 references. The complex mode indicator function (CMIF) of the HPS matrix is shown in Fig. 5 for two cases: (a) isotropic rotor with no gravity and (b) anisotropic rotor with $k_C = 0.97$ and gravity. There are two dominant singular value peaks in the CMIF with very close natural frequencies centered around 0.88 Hz. All of the other peaks, except for the peak at 1.8 Hz, are spaced at $n \times 0.16$ Hz from the peaks at 0.88 Hz. This indicates that the system has three modes that dominate this frequency range, two of which have noticeable periodic behaviour.

Fig. 5. CMIF of the HPS matrix for the 5 outputs using $\phi 1$, $\phi 2$, $\phi 3$ as references

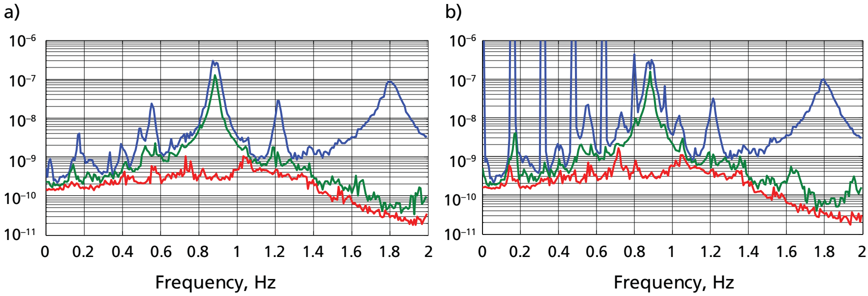

Initially, a simple output-only extension of the algorithm of mode isolation (AMI) is used to curve-fit the measurements. This gives a reasonable fit at all of the peaks, but AMI does not include the multiple-input/multiple-output (MIMO), hybrid approach [22, 23] that is necessary to separate modes that have close natural frequencies. Hence, the only mode retained from AMI is the mode at 1.801 Hz, which is found to be the first collective mode of the rotor. The two close modes are estimated using frequency domain decomposition (FDD) [24]. Specifically, the spectra near the peak are collected and a singular value decomposition (SVD) is used to extract the first three dominant singular vectors. These are used to condense the measurements to a set of three spectra as shown in Fig. 6. This spatial condensation of the measurements effectively separates the two close modes so that a simple single-mode fit can be applied to each curve to estimate the modal parameters. The natural frequencies and damping for the three rotor modes are given in Table 2, and the magnitude of the Fourier components are shown in Fig. 10 (a) and (c).

Fig. 6. Spatially condensed MIMO measurements

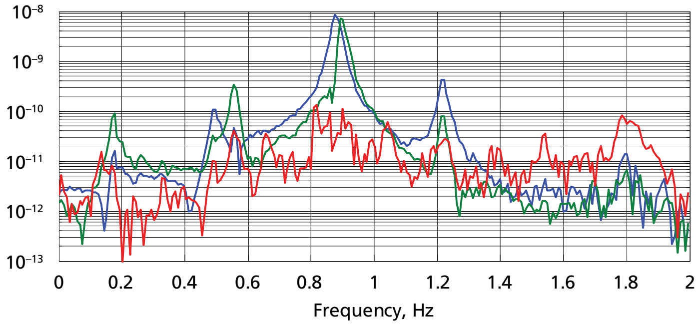

The next case considered is the case with gravity and 3% anisotropy in one of the blades. Again, AMI identifies the collective mode at 1.79 Hz, while FDD identifies the other two modes. The modal parameters are given in Table 2, and the mode shapes are in Fig. 10 (e) and (g).

These results illustrate what can be done with a basic system identification method based on HPS, and focus on the time-periodic blade modes. More sophisticated frequency-domain methods are advisable to use, such as the AFPoly algorithm [25] or pLSCF [26].

3.2.2 Results from H-OMA-TD

The response time histories obtained from modulation become input for the H-OMA-TD algorithm. Fig. 7 sketches how the method is applied using Brüel & Kjær OMA software Type 7760.

Fig. 7. Flow of the suggested method

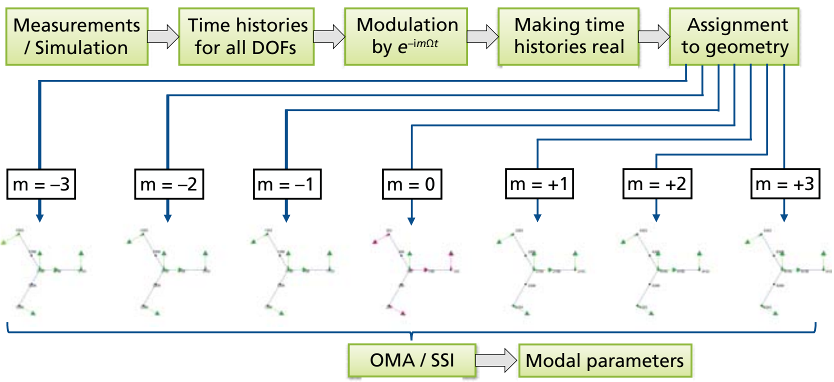

First, the data set of time histories for all six DOFs from the simulation (or from measurements) is harmonically modulated using $m = -3\ldots+3$, thus generating six new data sets. The new complex time histories are converted to real time using the algorithm described in section 2.2. With OMA software, six copies of the rotor geometry are constructed and assigned to the modulated data sets of the copies (Fig. 7). The unmodulated signals ($m = 0$) are selected as projection channels (shown in pink). Then a standard OMA procedure is run using data driven OMA/SSI with unweighted principal components (UPC), which extracts the modes.

A CMIF and a fragment of the stabilization diagram for the isotropic rotor in the absence of gravity are shown in Fig. 8. In the range 0 – 1.5 Hz, OMA finds nine modes. However, they are shifted ($\pm\Omega$) realizations of the three structural periodic modes: Horizontal, BW and FW. This is clearly seen when examining the mode shapes. Those corresponding to the BW mode are shown in the insets.

Fig. 8. Fragment of the stabilization diagram (Brüel & Kjær Type 7760 OMA software) showing horizontal, BW and FW modes of an isotropic rotor with no gravity

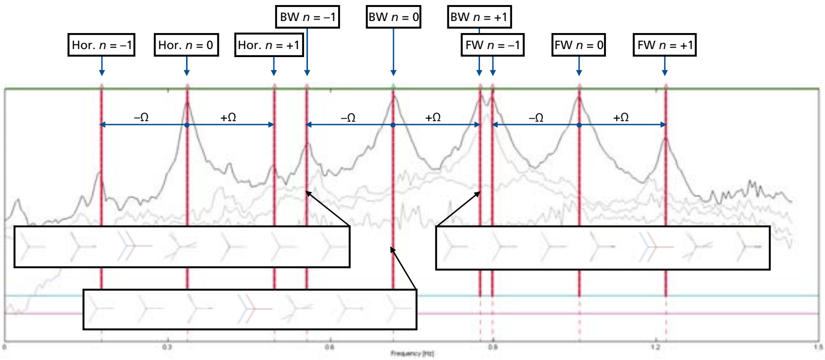

Table 2 explains the interpretation of the mode shapes using the BW mode as an example. The rows in the table correspond to the modes found by OMA/SSI (see Fig. 8). The middle row (BW, $n = 0$) shows that the periodic mode consists of three Fourier components oscillating at different frequencies: the horizontal component at 0.72 Hz, backward whirling component at 0.88 Hz and very weak forward whirling component at 0.56 Hz. Upon inspection, it can be seen that the top and bottom rows show the same components at the same frequencies.

Table 2. Isotropic rotor with no gravity. Shapes of the Fourier components for BW mode for different n

Name	Frequency, Hz	Mode Shape						
		***m* = –3**	***m* = –2**	***m* = –1**	***m* = 0**	***m* = +1**	***m* = +2**	***m* = +3**
BW, *n* = –1	0.56							
		0.56 − 3Ω = 0.08 Hz	0.56 − 2Ω = 0.24 Hz	0.56 − Ω = 0.40 Hz	0.56 Hz	0.56 + Ω = 0.72 Hz	0.56 + 2Ω = 0.88 Hz	0.56 + 3Ω = 1.04 Hz
BW, *n* = 0	0.72							
		0.72 − 3Ω = 0.24 Hz	0.72 − 2Ω = 0.40 Hz	0.72 − Ω = 0.56 Hz	0.72 Hz	0.72 + Ω = 0.88 Hz	0.72 + 2Ω = 1.04 Hz	0.72 + 3Ω = 1.20 Hz
BW, *n* = +1	0.88							
		0.88 − 3Ω = 0.40 Hz	0.88 − 2Ω = 0.56 Hz	0.88 − Ω = 0.72 Hz	0.88Hz	0.88 + Ω = 1.04 Hz	0.88 + 2Ω = 1.20 Hz	0.88 + 3Ω = 1.36 Hz

Note that the phase relationships between the DOFs are only valid inside each Fourier component and do not make sense between the components.

The values of the Fourier exponents are given in Table 1. The magnitude of the Fourier components are shown in Fig. 2 (b) and (d), and Fig. 3 (d), (e) and (f). They are compared with the results of analytical Floquet analysis. The frequencies, damping and mode shapes agree with the analytical values.

Fig. 3 explains the results of H-OMA-TD in detail using the BW mode as an example. The simulation is conducted for five different realizations of the excitation input, and system identification is performed for each realization. Fig. 3 (b), (d) and (f) show the mean magnitudes of the obtained Fourier components; the confidence bounds on the results based on the five observations are also shown. Although the H-OMA-TD algorithm produces many Fourier components, it can be seen that the confidence of the noise components is significantly lower (the confidence band is wider), and the false components can be readily identified and filtered out. The true components are shown inside the dotted regions of Fig. 3 (b), (d) and (f), and coincide with the analytical results obtained via Floquet analysis. Fig. 3 (e) shows the scatter of the shape of the BW and FW Fourier components (compare with the analytical plots in Fig. 3 (a)).

Fig. 4 compares the results of Floquet analysis with the results of H-OMA-TD for the anisotropic rotor in the presence of gravity. Dotted lines surround the regions where the H-OMA-TD method catches the Fourier components well. These components dominate the dynamics of the mode, while the others are significantly lower in magnitude. The dashed line in Fig. 4 (b) indicates the erroneous components that do not show up in the analytical solution (Fig. 4 (a)). These components can be explained by the strong influence of the rotor harmonics nearby the component frequencies (see the strong peaks in Fig. 5 (b)). Table 1 provides the Floquet exponents and compares them with the analytically obtained ones; both agree quite well.

The complexity plots in Fig. 9 compare the dominating Fourier components for the two whirling modes. The anisotropic property of the rotor causes the asymmetry of the shapes. Despite the scatter, this observed asymmetry can be used as an indicator of damage. Notice that the stiffness of Blade 3 is reduced by 3%. This information may also be used to localize the damage [18].

*Fig. 9. Complexity plots for an anisotropic rotor. Blade 3 has a 3% reduction in stiffness. For the BW mode, the BW (dominating) component: **a**) exact solution, **b**) the H-OMA-TD results for five simulated experiments. For the FW mode, the FW (dominating) component: **c**) exact solution, **d**) the H-OMA-TD results for five experiments*

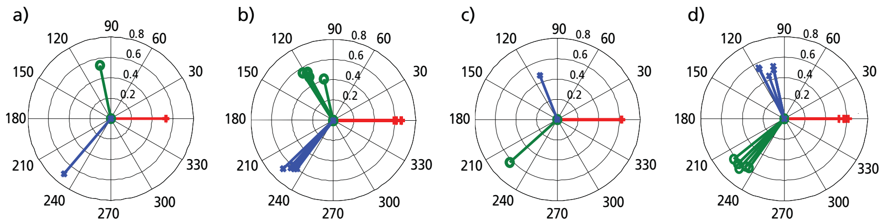

3.2.3 Result Comparison

Table 1 shows the analytically obtained Floquet exponents and compares them with the frequencies found by H-OMA methods in the time and frequency domain. If damping is to be characterized with a damping ratio, then the value of the ratio depends on the chosen natural frequency. The latter is not invariant since a shift by an integer multiplier of Ω is also a natural frequency (Table 2). However, the real part of the Floquet multipliers is invariant, and can be used to characterize the damping and system stability.

Fig. 10. Magnitudes of modal components obtained by H-OMA-FD (left column) and H-OMA-TD (right column). Isotropic rotor in the absence of gravity: a,b) BW mode, c,d) FW mode. Anisotropic rotor in the presence of gravity: e,f) BW mode, g,h) FW mode

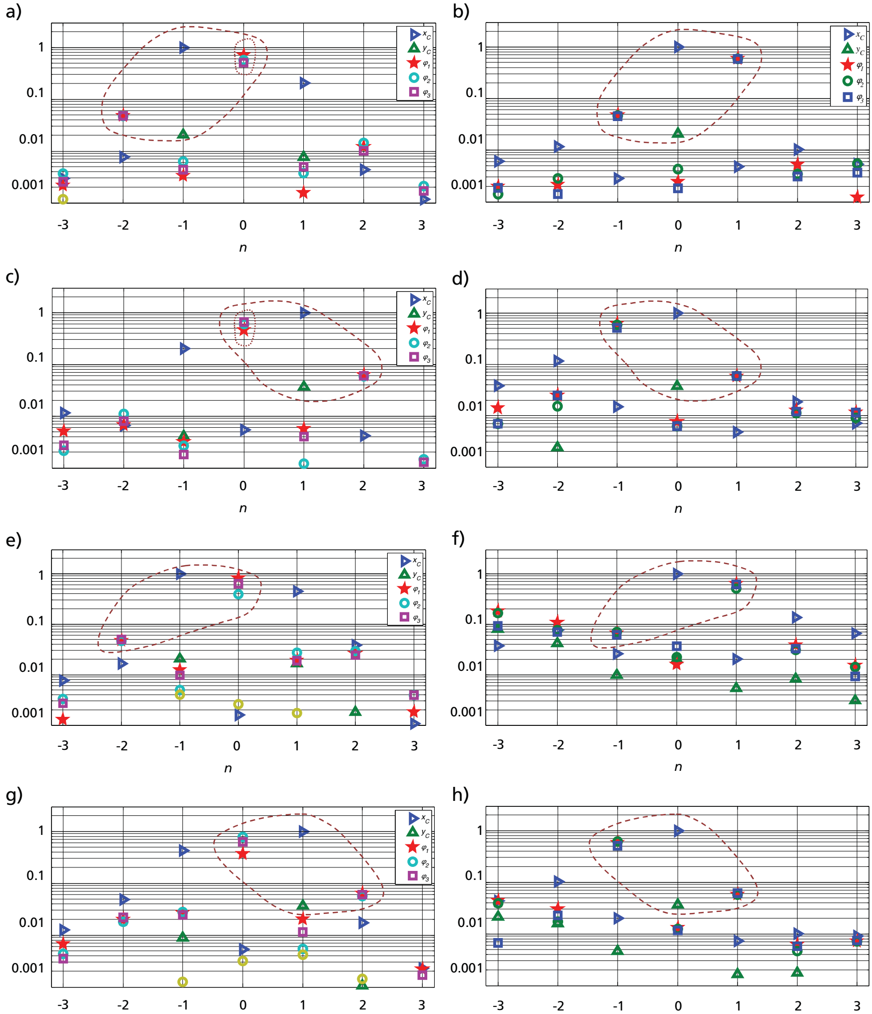

Fig. 10 compares the magnitudes of the modal components of BW and FW modes obtained by frequency and time domain methods for both the isotropic rotor in the absence of gravity, Fig. 10 (a) through (d), and the anisotropic rotor when gravity is present, Fig. 10 (e) through (h). The dominant components of the modes are outlined by dashed lines. Observe that the two methods provide similar results, though the frequency domain results are slightly incorrect when reporting the different magnitudes of $\phi 1$, $\phi 2$, $\phi 3$ for the isotropic case (outlined by dotted lines). This might be improved by using a multi-reference technique. The same can be said regarding the phase. The natural frequencies reported by the two methods differ by Ω, which is natural for periodic systems. Actually, the mode shown in Fig. 10 (a) is comparable with the representation of a BW isotropic rotor with no gravity and $n = +1$ in Table 2.

It is also interesting to compare the results of H-OMA-TD with the results from the direct application of OMA to the measured data, thus ignoring the fact that the system is LPTV; an approach used in [18]. In the framework of the H-OMA-TD method, it means narrowing the range of m in Eq. (11) to 0. As it follows from Table 2, it is still possible to extract the Fourier components (each mode found will be a Fourier component). If the LPTV nature of the system is recognized, the mode has to be manually assembled from the found Fourier components, knowing that they are separated by integer multipliers of Ω. It is also important to note that the mutual scaling of the Fourier components is lost in this case.

4. Conclusion and Future Research

This study suggests a simple method of extending existing implementations of time domain OMA SSI algorithms to time-periodic systems. The method consists of two steps: harmonically modulate the experimentally obtained time histories (multiply by $e^{-\mathrm{i}m\Omega t}$) and make the obtained complex time histories real. The preprocessed data becomes input for the standard OMA algorithm. In addition, the authors give some advice on how to prepare the data for OMA in order to interpret the results more easily.

The method is demonstrated on synthesized data obtained via simulation of a simple 3-bladed rotor that is subjected to random noise excitation. The results of this simulated experiment are validated against the analytical results from Floquet analysis and the results provided by the conventional HPS method implemented in the frequency domain. The suggested algorithm avoids manual peak picking and allows for automation, which can be useful in structure health monitoring systems.

The suggested method originates from engineering practice and requires a strong mathematical foundation. Mode shape normalization and scaling when using acceleration measurements as well as estimation of damping ratios need to be addressed. Application of the method to real measurements from a wind turbine is a natural next step.

Acknowledgements

The work is partly supported by the Danish Energy Technology Development and Demonstration Programme (EUDP), grant number 64011-0084 "Predictive Structure Health monitoring of Wind Turbines".

References

[1] G. H. James, T. G. Carne, *Damping measurements on operating wind turbines using the natural excitation technique (NExT)*. In *Proceedings of 11th ASME Wind Energy Symposium presented at the Energy Sources Technology Conference and Exhibition*. Houston, USA (1992). Vol. 12, pp. 75-81.

[2] D. Tcherniak, S. Chauhan, M. Rossetti, I. Font, J. Basurko, O. Salgado. *Output-only Modal Analysis on Operating Wind Turbines: Application to Simulated Data*. In *Proceedings of European Wind Energy Conference*, Warsaw, Poland (2010).

[3] A. Jhinaoui, *Subspace-based identication and vibration monitoring algorithms for rotating systems*, PhD Thesis, Rennes, France (2014).

[4] M.S. Allen, *Frequency-Domain Identification of Linear Time-Periodic Systems using LTI Techniques*, Journal of Computational and Nonlinear Dynamics, Vol. 4, No. 4 (2009).

[5] M.S. Allen, M. W. Sracic, et al. *Output-Only Modal Analysis of Linear Time Periodic Systems with Application to Wind Turbine Simulation Data*, Mechanical Systems and Signal Processing Vol. 25 (2011), pp. 1174-1191.

[6] S. Yang, M. S. Allen, *A Lifting Algorithm for Output-only Continuous Scan Laser Doppler Vibrometry*, In *Proceedings of 53rd AIAA Structures, Structural Dynamics, and Materials Conference*, Honolulu, Hawaii (2012).

[7] S. Yang, M. S. Allen, *Output-Only Modal Analysis Using Continuous-Scan Laser Doppler Vibrometry and Application to a 20kW Wind Turbine*, Mechanical Systems and Signal Processing Vol.31 (2012), pp. 228–245.

[8] S. Yang, M. S. Allen, *Transfer Functions to Measure Translational and Rotational Velocities with Continuous-Scan Laser Doppler Vibrometry*, In *Proceeding of 31st International Modal Analysis Conference (IMAC XXXI),* Garden Grove, CA, USA (2013).

[9] S. Yang, M. S. Allen, *Harmonic Transfer Function to Measure Translational and Rotational Velocities With Continuous-Scan Laser Doppler Vibrometry*, Journal of Vibration and Acoustics, Vol. 136, No. 2, (2014).

[10] S. Yang, S., D. Tcherniak, M. S. Allen, *Modal Analysis of Rotating Wind Turbine using Multi-blade Coordinate Transformation and Harmonic power spectrum*, In *Proceedings of 32nd International Modal Analysis Conference (IMAC XXXII)*, Orlando, FL, USA (2014).

[11] J. H. Ginsberg, *Mechanical and Structural Vibrations*, New York, John Wiley and Sons (2001).

[12] C. Chen, *Linear Systems Theory and Design*, New York, Oxford University Press, Inc. (1999).

[13] N. M. Wereley, *Analysis and Control of Linear Periodically Time Varying Systems*, PhD Thesis, Massachusetts Institute of Technology, (1991).

[14] G. Floquet, *Sur Les Equations Lineairs a Coefficients Periodiques*, Ann. Sci. Ecole Norm. Sup., Vol. 12, (1883) pp. 47-88.

[15] P. Hartman, *Ordinary Differential Equations*, New York, John Wiley & Sons, Inc. (1964).

[16] J. Guckenheimer, P. Holmes, *Nonlinear Oscillations, Dynamical Systems, and Bifurcations of Vector Fields*, New York, Springer-Verlag New York Inc. (1983).

[17] H. Hochstadt, *Differential Equations*, New York, Dover (1964).

[18] D. Tcherniak, *Loss of Rotor Isotropy as a Blade Damage Indicator for Wind Turbine Structure Health* Monitoring Systems, In *Proceedings of European*

Workshop on Structure Health Monitoring (EWSHM), Nantes, France (2014).

[19] P. F. Skjoldan, *Aeroelastic modal dynamics of wind turbines including anisotropic effects*, PhD Thesis, Roskilde, Denmark (2011).

[20] M. H. Hansen, *Improved Modal Dynamics of Wind Turbines to Avoid Stall-induced Vibrations*, Wind Energy, Vol. 6 (2003), pp.179-195

[21] D. Tcherniak, S. Chauhan, M. N. Hansen, *Applicability Limits of Operational Modal Analysis to Operational Wind Turbines*, In *Proceedings of 28th Int. Modal Analysis Conference (IMAC)*, Orlando, FL, USA (2010).

[22] M.S. Allen, *Global and Multi-Input-Multi-Output (MIMO) Extensi ons of the Algorithm of Mode Isolation (AMI)*, Doctorate, Georgia Institute of Technology (2005).

[23] M. S. Allen, J. H. Ginsberg, *Global, Hybrid, MIMO Implementation of the Algorithm of Mode Isolation*, In *Proceedings of 23rd International Modal Analysis Conference (IMAC XXIII)*, Orlando, FL, USA (2005).

[24] R. J. Allemang, D. L. Brown, *A Unified Matrix Polynomial Approach to Modal Identification*, Journal of Sound and Vibration, Vol. 211, No. 3 (1998), pp. 301-322.

[25] H. Vold, K. Napolitano, et al, *Aliasing in modal parameter estimation: An historical look and new innovations*, In *Proceedings of 25th Internatio nal Modal Analysis Conference*, Orlando, FL, USA (2007).

[26] P. P. Guillaume, P. Verboven, et al., *A Poly-Reference Implementa tion of the Least-Squares Complex Frequency-Domain Estimator*, *In Proccedings of International Modal Analysis Conference (IMAC XXI)*, Kissimmee, FL, USA (2003).

Microphone Acoustic Impedance in Reciprocity Calibration of Laboratory Standard Microphones*

Erling Sandermann Olsen† *and Erling Frederiksen*‡

Abstract

Primary calibration of laboratory standard microphones with the reciprocity technique is standardized in international standard, IEC Publication 61094-2:2009. The standard describes how to calculate the acoustical transfer impedance between pairs of microphones mounted in standardized couplers. As stated in the standard, the acoustic impedances of the microphones form an important part of the acoustic transfer impedance of the system. However, the standard only describes how to determine a first approximation of the acoustic impedance expressed as a three-component lumped parameter model with mass, compliance and resistance in series. In this paper it is demonstrated that a better representation of the microphone acoustic impedance is immediately available and that the lumped parameter model is too simple. It is shown that the frequency dependence of the acoustic impedance of the microphones is closely related to the sensitivity of the microphones. Therefore, the frequency dependence can be determined with an iterative procedure, but the absolute level has to be determined separately. The influence on calibration uncertainty of using the improved impedance representation and the determination of the absolute level of the acoustic impedance of the microphones are discussed.

Résumé

L'étalonnage primaire des microphones étalons de laboratoire par réciprocité est décrite par la Publication CEI 61094-2:2009. Cette norme décrit le mode de

---

* First published at INTER-NOISE 2013, Innsbruck, Austria

† Brüel & Kjær Sound & Vibration A/S, Denmark

‡ ef-consult, Denmark

détermination de l'impédance acoustique de transfert entre deux microphones montés sur des coupleurs normalisés. Comme le précise cette norme, les impédances acoustiques des microphones constituent une part importante de l'impédance de transfert du système. Toutefois, elle ne décrit que la manière d'obtenir une première approximation de cette impédance, exprimée par un modèle paramétrique grossier à trois composantes, avec masse, compliance et résistance en série. Il est démontré ici qu'une meilleure représentation de l'impédance acoustique des microphones est possible et que le modèle paramétrique est trop simpliste. Il est montré que la dépendance en fréquence de l'impédance acoustique des microphones est étroitement liée à la sensibilité de ces capteurs, et qu'elle peut donc être déterminée au moyen d'une procédure itérative, tandis que le niveau en valeur absolue doit être déterminé séparément. Sont également discutées l'influence d'une représentation améliorée de l'impédance sur l'incertitude de l'étalonnage ainsi que la détermination du niveau absolu de l'impédance acoustique des microphones.

Zusammenfassung

Die Primärkalibrierung von Laboratoriums-Normalmikrofonen nach dem Reziprozitätsverfahren ist in der internationalen Norm IEC 61094-2:2009 standardisiert. Die Norm beschreibt, wie die akustische Übertragungsimpedanz zwischen Mikrofonpaaren berechnet wird, die in standardisierten Kupplern montiert sind. Gemäß der Norm stellen die akustischen Impedanzen der Mikrofone einen wichtigen Teil der akustischen Übertragungsimpedanz des Systems dar. Die Norm beschreibt jedoch nur, wie eine erste Näherung der akustischen Impedanz bestimmt wird, ausgedrückt als dreikomponentiges Lumped-Parameter-Modell mit Masse, Nachgiebigkeit und Widerstand in Reihe. In diesem Artikel wird nachgewiesen, dass das Lumped-Parameter-Modell zu einfach ist und eine bessere Darstellung der akustischen Impedanz der Mikrofone unmittelbar zur Verfügung steht. Es wird gezeigt, dass die Frequenzabhängigkeit der akustischen Mikrofonimpedanz in engem Zusammenhang mit der Empfindlichkeit der Mikrofone steht. Deshalb kann die Frequenzabhängigkeit mit einem iterativen Verfahren ermittelt werden, während der absolute Wert separat bestimmt werden muss. Es wird der Einfluss der besseren Impedanzdarstellung auf die Kalibrierunsicherheit und die Bestimmung des Absolutwertes der akustischen Impedanz der Mikrofone diskutiert.

1. Introduction

As of today, the primary standard for sound pressure level is defined indirectly through the sensitivity of laboratory standard, LS, microphones. The capability of measuring sound pressure therefore depend on the uncertainty of measurement of the absolute sensitivity of LS microphones and of the methods used to transfer the sensitivity to sound measuring devices such as sound level meters and couplers used for audiometer and telephone measurements. In order to be able to calibrate sound measuring devices for use in different sound fields, it is necessary to know the pressure sensitivity as well as the free-field sensitivity of LS microphones. The subject of this paper is reciprocity calibration of pressure sensitivity of LS microphones, and in particular the calculation of the acoustic admittance of the diaphragms of the microphones being calibrated.

Primary pressure sensitivity calibration of laboratory standard microphones with the reciprocity technique is standardized in international standard, IEC Publication 61094 2:2009 [1], IEC 61094-2 for short. In IEC 61094-2 it is described how to calculate the acoustical transfer impedance between pairs of microphones mounted in standardized couplers. However, the standard is open for interpretation on some points. The methods for calculation of corrections for heat conduction and viscous losses have been discussed in a previous paper [2]. It is suggested in the standard that the admittance of the microphone diaphragm is calculated with a simple lumped parameter representation. It is however also mentioned that the diaphragm compliance increases towards lower frequencies, but it is not clear whether it is recommend or not to include it in the calculations. As shown in the previous paper this has an influence on the results and on the interpretation on other parts in the standard.

In this paper the calculation of the admittances of the microphone diaphragms is discussed. A new representation of the admittances is proposed. The influence of the measurement results and uncertainty of measurement is discussed and it is also proposed that the representation can be used in a simplified calibration procedure for laboratories that whishes to make calibrations with a single coupler.

It is assumed for the calculations made for this paper that the radial wave motion correction recommended in IEC 61094-2 is valid. The correction applied for heat conduction and viscosity is the low frequency solution for low frequencies and the broad band solution for high frequencies with a gradual transition at medium frequencies.

2. Microphone Admittances in Reciprocity Calibration

The acoustic admittances of the microphone diaphragms are parts of the acoustic transfer impedance of the coupler with the microphones, cf. equations (3) and (4) of IEC 61094-2 [1]. It is recommended in the standard to express the impedance (the reciprocal of the admittance) of each microphone in terms of an equivalent series connection of compliance, mass and resistance. To the knowledge of the authors, as of today this is the dominant model used in the context of calculation the transfer admittance of couplers in reciprocity calibrations, if not the only one. Although it is mentioned that the compliance increases towards lower frequencies, that is not treated further in the standard and it is stated that the model is valid up to 1.3 times the resonance frequency.

For the purpose of this paper, the acoustic admittance of a microphone, Y, is separated into a fixed value, Y_0, at a reasonably chosen frequency, f_0, so that $Y_0 = Y(f_0)$ and its frequency dependence:

$$Y = Y_0 \frac{Y}{Y_0} \tag{1}$$

These two parts may be determined independently.

It is proposed that, instead of a assuming a specific model of the acoustic admittance of a microphone, the frequency dependence of the admittance is assumed to be the same as that of the sensitivity and the fixed value can be found or known from separate measurement or knowledge, i.e.:

$$Y = Y_0 \frac{S}{S_0} \tag{2}$$

where S_0 is the sensitivity at the frequency f_0. With this approach and provided that the fixed values are available, the acoustic admittances of the microphones in reciprocity calibration can be determined with an iterative procedure, even when only a single coupler is used for calibration in the full frequency range.

Below, it is discussed how well the frequency dependence of the sensitivity represents the frequency dependence of the admittance, and it is discussed how to obtain the fixed value and whether the approach constitutes an improvement as compared to the simple model used today.

3. Microphone Acoustic Admittance and Sensitivity

Laboratory standard microphones are traditional condenser microphones where the metallic diaphragm and the backplate form a capacitor that is charged to a predetermined voltage, V_{p}. Here it is assumed that the charge is constant during operation. When the microphone is exposed to sound, the movement of the diaphragm leads to changes in the capacitance and to corresponding (open circuit) voltage variations:

$$u = \frac{Q}{C} - \frac{Q}{C_0} = \frac{V_{\mathrm{p}} C_0}{C} - V_{\mathrm{p}} = V_{\mathrm{p}} \frac{C_0 - C}{C} \tag{3}$$

The pressure sensitivity is the ratio of the output voltage to a uniform pressure, p, over the diaphragm surface [3]:

$$S = \frac{u}{p} = \frac{1}{p} V_{\mathrm{p}} \frac{C_0 - C}{C} \tag{4}$$

The acoustic admittance of the diaphragm is the ratio of the volume velocity, q, of the diaphragm and the uniform pressure

$$Y = \frac{q}{p} \tag{5}$$

In the following only the capacitance formed by the diaphragm directly over the backplate is considered. Stray capacitances and the influence of passive capacitances, such as the capacitance of the microphone housing and the input capacitance of the preamplifier, as well as the influence of electrostatic attraction forces are ignored here. These simplifications are considered reasonable for the purpose of this paper where laboratory standard microphones in pressure sensitivity reciprocity calibration are considered.

Consider first a very simple model of the microphones where the diaphragm is considered a moving piston. The capacitance is:

$$C = \varepsilon \frac{S_{\mathrm{b}}}{d} = \varepsilon \frac{S_{\mathrm{b}}}{d_0 + x} \tag{6}$$

where S_b is the surface area of the backplate, d is the distance between the diaphragm and the backplate and ε is the permittivity of the air in the gap.

The admittance is:

$$Y = \frac{q}{p} = \frac{S_\mathrm{d} x}{p} \tag{7}$$

where S_d is the surface area of the diaphragm.

The sensitivity is:

$$S = \frac{V_\mathrm{p}}{p}\frac{C_0 - C}{C} = \frac{V_\mathrm{p}}{p}\frac{\frac{1}{d_0} - \frac{1}{d_0 + x}}{\frac{1}{d_0 + x}} = \frac{V_\mathrm{p}}{p}\left(\frac{d_0 + x}{d_0} - 1\right) = \frac{V_\mathrm{p}}{p}\frac{x}{d_0} = Y\frac{V_\mathrm{p}}{S_0 d_0} \tag{8}$$

The admittance is:

$$Y = \frac{q}{p} = \frac{S_\mathrm{d} x}{p} = S\frac{S_\mathrm{d} d_0}{V_\mathrm{p}} \tag{9}$$

Thus, in the simple case where the diaphragm is assumed to move like a piston the admittance is proportional to the sensitivity. This observation was the starting point for the considerations presented in this paper.

The diaphragm of a microphone does, however, not move as a piston, and in the general case the deflection pattern, $x(\mathbf{r})$, where x is the deflection and $\mathbf{r}$ is the position on the diaphragm, is not known. In the general case the voltage generated on the backplate is (note, integration over backplate surface):

$$S = \frac{V_{\mathrm{p}}}{p} \frac{\int\limits_{S_{\mathrm{b}}} \varepsilon \frac{1}{d_0} dA - \int\limits_{S_{\mathrm{b}}} \varepsilon \frac{1}{d_0}\left(1 - \frac{x(\mathbf{r})}{d_0 + x(\mathbf{r})}\right) dA}{\int\limits_{S_{\mathrm{b}}} \varepsilon \frac{1}{d_0}\left(1 - \frac{x(\mathbf{r})}{d_0 + x(\mathbf{r})}\right) dA}$$

$$S = \frac{V_{\mathrm{p}}}{p} \frac{\int\limits_{S_{\mathrm{b}}} dA - \int\limits_{S_{\mathrm{b}}} \left(1 - \frac{x(\mathbf{r})}{d_0 + x(\mathbf{r})}\right) dA}{\int\limits_{S_{\mathrm{b}}} \left(1 - \frac{x(\mathbf{r})}{d_0 + x(\mathbf{r})}\right) dA} \tag{10}$$

$$S = \frac{V_{\mathrm{p}}}{p} \frac{S_{\mathrm{b}} - S_{\mathrm{b}} + \int\limits_{S_{\mathrm{b}}} \frac{x(\mathbf{r})}{d_0 + x(\mathbf{r})} dA}{S_{\mathrm{b}} - \int\limits_{S_{\mathrm{b}}} \frac{x(\mathbf{r})}{d_0 + x(\mathbf{r})} dA} \approx \frac{V_{\mathrm{p}}}{p} \frac{\frac{1}{d_0} \int\limits_{S_{\mathrm{b}}} x(\mathbf{r}) dA}{S_{\mathrm{b}}}$$

The approximation in the last term is made under the assumption that the displacement of the diaphragm is very small as compared to the equilibrium distance, d_0. Under that assumption the output voltage is proportional to the volume displacement of the part of the diaphragm that is over the backplate.

The diaphragm admittance is the ratio of the volume displacement of the entire diaphragm to the (uniform) sound pressure (note, integration over diaphragm surface):

$$Y = \frac{q}{p} = \frac{\int\limits_{S_{\mathrm{d}}} x(\mathbf{r}) dA}{p} \tag{11}$$

Thus, the relation between the admittance and the sensitivity in the general case for small displacements is:

$$Y = S\frac{d_0 S_\mathrm{b}}{V_\mathrm{p}} \frac{\int_{S_\mathrm{d}} x(\mathbf{r})dA}{\int_{S_\mathrm{b}} x(\mathbf{r})dA} \tag{12}$$

In frequency ranges where the displacement pattern of the diaphragm is unchanged, the ratio of the two volume displacements will be the same, and thereby the admittance will be proportional to the sensitivity. This is likely to be the case at low frequencies where the diaphragm deflection can be assumed to be quasi-stationary. At higher frequencies the deflection pattern is complicated and depends on details in the microphone construction, and it is therefore not possible to determine the ratio in general terms.

4. Investigations with Numerical Modeling

In order to determine the ratio between the volume displacement of the whole diaphragm to that of the part of the diaphragm over the backplate the deflection pattern must be known in some way. For the purpose of this paper the deflection pattern has been calculated using numerical modeling.

The numerical model used for the investigations is developed using the finite element method with COMSOL Multiphysics® [4] in collaboration between COMSOL and Brüel & Kjær. The model includes description of the electric, mechanic, and acoustic properties of the microphone back cavity and diaphragm, including thermal and viscous losses of the air inside the microphone [5]. The model has been adapted to LS2P microphone, Brüel & Kjær Type 4180, and, with slight simplification (so as to limit calculation resource requirements), to LS1P microphone, Brüel & Kjær Type 4160.

Below it is shown based on the model at which frequencies the proportionality is a good approximation, and it is discussed whether the simple lumped parameter model of the standard or assumed proportionality with the sensitivity is the preferable admittance model at higher frequency.

In Fig. 1 the frequency dependence of the sensitivity, the admittance, the volume displacement over the backplate, and the lumped parameter model are shown for LS1P and LS2P microphones, all normalized to their minimum value at frequencies below the resonance frequency. Note that the curves for the sensitivity and the displacement over the backplate practically speaking coincide.

Fig. 1. Normalized level of admittance, sensitivity, volume displacement over backplate calculated with numeric model and admittance calculated with the lumped parameter model a: LS1 microphone b: LS2 microphone

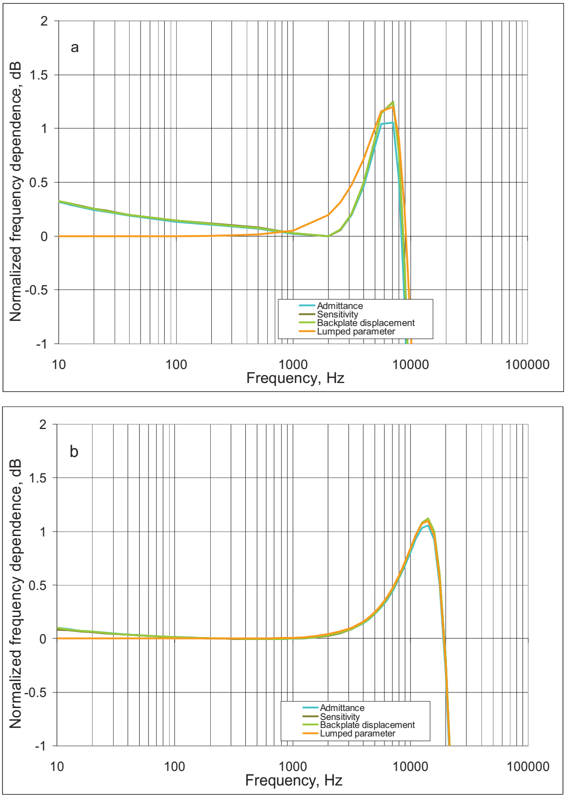

130758

In Fig. 2 the same data are shown in a way that illustrates the differences. The normalized frequency dependence of the sensitivity, the volume displacement over the backplate, and the lumped parameter model are shown relative to the normalized admittance. Note that the normalization is somehow arbitrary. The match is not necessarily best at zero, but where the slopes are closest.

Fig. 2. Normalized level of sensitivity and volume displacement over backplate calculated with numeric model and admittance calculated with the lumped parameter model relative to the admittance calculated with numeric model. a: LS1 microphone b: LS2 microphone

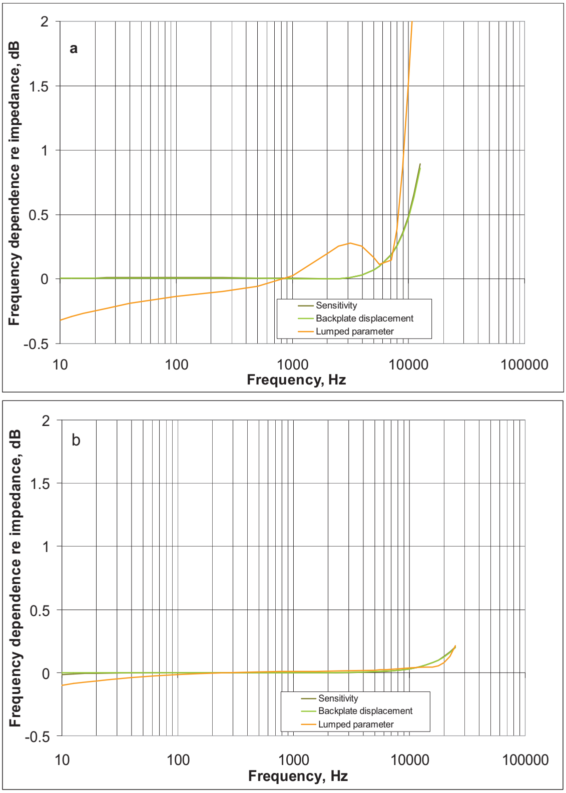

130759

Figures 1 and 2 clearly show that at low frequencies the frequency dependence of the microphone admittance follows that of the sensitivity. For LS1 microphones it is also a better representation of the admittance at higher frequencies, whereas the frequency dependence of the sensitivity and the lumped parameter model seem to be equally adequate for LS2 microphones. At high frequencies the lumped parameter model as well as the proposed model overestimates the admittance of the diaphragm. The figures also clearly demonstrate the validity of the approximation in equation (11), as the sensitivity and the volume displacement over the backplate have practically speaking exactly the same frequency dependence.

Thus, if the value of the admittance is known at one frequency, the combination of this fixed value and the frequency dependence of the sensitivity will in general be a better approximation to the admittance than the lumped parameter model, in particular at low frequencies. The fixed value must, however, be found in some way, and as shown below it is essential for the final result that the value is correct.

5. Determination of the Fixed Value

As seen in Fig. 2, at intermediate frequencies the frequency dependence of the lumped parameter model to a reasonable degree matches that of the numerically calculated admittance and sensitivity. The match is indeed, however, better for LS2 microphones than for LS1 microphones. One way to determine the fixed value is therefore to use the same methods used hitherto for determination of the parameters in the lumped parameter model [1, 6, 7] to find the first approximation of the admittance. The frequency range used should be limited to the range where the match is reasonable. The admittance of the lumped parameter model in the center of the frequency range used can then be applied as the fixed value, Y_0, in equation (2).

The method used to determine the fixed value depends on the number of couplers that are used for the measurements. As the methods are well know and well established, they are only briefly summarized here.

Note that in the context of this paper it is assumed that the total volume, i.e. the combined admittance of the front cavity volume and the equivalent volume part of the microphone admittance, is known with high accuracy. The total volume can be determined at medium frequencies with at least two couplers. If the equivalent volume is changed in the calculation of the fixed impedance, the front volume of the microphone must be changed correspondingly in order to keep the effective volume unchanged. As the low frequency variation of the microphone admittance is taken into account, the admittance representation presented here also leads to a more correct determination of the front volume of the microphones in the two following methods [2].

Many laboratories around the world use the Brüel & Kjær Reciprocity Calibration System Type 9699 [7]. In its standard configuration the calibration system comes with a pair of plane wave couplers for each of LS1 and LS2 microphones. One of the couplers in each pair has dimensions that minimizes the influence of radial wave motion and can be used at frequencies up to the first asymmetrical mode of the couplers. The other coupler in each pair is long so as to achieve a high volume and can only be used up to a few kilohertz. The total volume can be determined by minimizing the difference of the results at medium frequencies with the two couplers, the loss factor can be derived from the measured response and the resonance frequency is the frequency of 90° phase shift in the sensitivity. As only one of each pair can be used in the full frequency range of the microphones, there is no way to see whether the sensitivity result at high frequencies depends on the coupler size. In that case the value of the equivalent volume must be estimated from the total volume and the geometrical volume of the front cavity.

Some laboratories use two or more, typically four, couplers that can be used in the full frequency range of the calibrations for each of LS1 and LS2 microphones. Together with the shorter of the couplers mentioned above, Brüel & Kjær Coupler Sets WZ-0078 and WZ-0079 [8] form such sets of four couplers. The dimensions of the four couplers for each of LS1 and LS2 cover the range recommended in Annex C in IEC 61094-2 and they can all be used at frequencies up to the first asymmetrical mode. With more than one coupler covering the full frequency range it is possible to estimate the total volume by minimizing the differences between the results in the four different couplers at low and medium frequencies and the parameters for calculation of the fixed point (using the the lumped parameter model) by minimizing the differences around the resonance frequency [6].

6. Influence on Results and Uncertainty

In order to investigate the significance of changing to the proposed representation of the microphone admittance in reciprocity calibrations, the difference between the lumped parameter model and the proposed representation is investigated.

In Fig. 3 the difference between results calculated with the lumped parameter admittance model and using the proposed model is shown for LS1 and LS2 microphones. The fixed point in the proposed model is the admittance of the lumped parameter model at $0.03 \cdot f_{\mathrm{res}}$. The parameters were determined so as to give the best match of results of four couplers with the lumped parameter model.

As of today uncertainty components in the order of 0.01 dB contributes significantly to the measurement of uncertainty in pressure sensitivity reciprocity calibrations [2]. At low and high frequencies the differences shown in Fig. 3 are of the same order of magnitude. Assuming that the proposed model is correct this

Fig. 3. Difference between results obtained using the proposed admittance representation and the lumped parameter model.

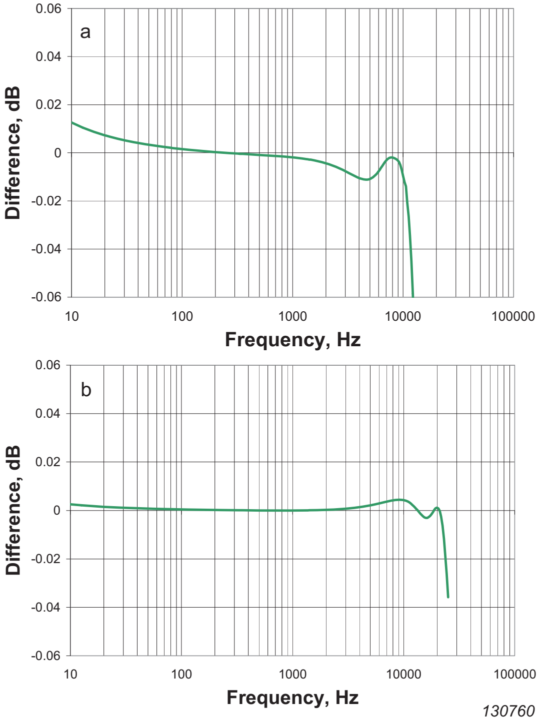

means the difference has been an overseen uncertainty component in pressure sensitivity calibrations and that the model must be applied in order to minimize the uncertainty. This is evidently the case for low frequencies. At high frequencies further validation of the method and investigation of the frequency range of validity may need to be investigated further. Until the proposed method is validated, the differences should be considered in calculations of uncertainty of measurement.

The importance of a correct fixed value is illustrated in Fig. 4 where the influence of changing the equivalent volume part of the fixed impedance by 15% in a calculation for a single coupler is shown. The influence is clearly very small at low and medium frequencies, but at the highest frequencies of interest the contribution to the measurement uncertainty should be considered. A variation of

15% of V_{eq} may seem exaggerated, but if the value is not determined from measurements at high frequencies in more than one coupler the uncertainty may reach that level. This is at present under further investigation by the authors.

Fig. 4. Influence of a change in Veq of 15% on results with the proposed admittance representation

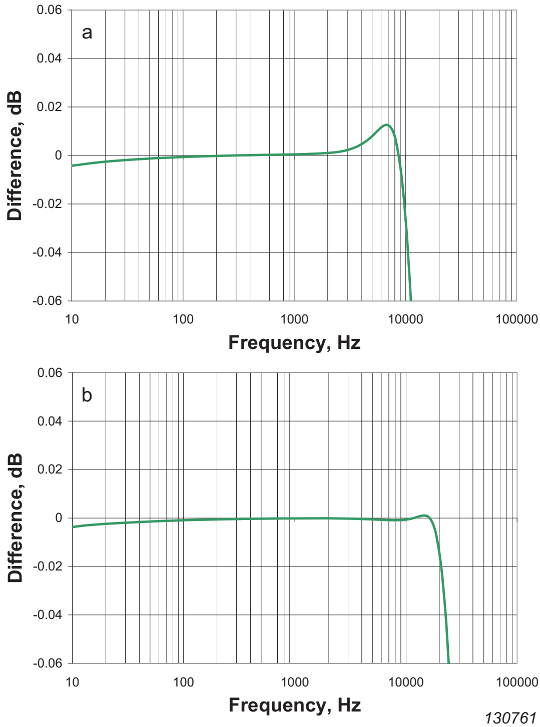

7. Application in Simple Calibration Procedure

The proposed method may be used to establish a simple procedure for calibration with a single coupler. The front volume of the microphone, V_f, and the compliance of the diaphragm expressed as its equivalent volume, V_{eq}, are assumed to be known, for example from manufacturer data or from a more comprehensive initial measurement. The calibration is made with the coupler in the usual way. The results are calculated first with the lumped parameter model using standard values of the resonance frequency, f_{res}, and the loss factor, d. Based on the result new values f_{res} and d are calculated as described above and the calculation is repeated using the new representation of the admittance with the fixed point calculated at a reasonable frequency, e.g., $0.03 \cdot f_{res}$ using the known values of V_f and V_{eq} and the new values of f_{res} and d.

8. Conclusions

In this paper the acoustic admittance of LS microphones have been discussed. The conclusions made are based on a new, detailed numerical model. The model is believed by the authors to sufficiently accurate to sustain the conclusions. Supplementary validation of the model is of course highly desirable. The conclusions are:

- An accurate and simple to find representation of the microphone admittance has been presented
- The complex admittance is to a good approximation proportional to complex sensitivity
- The admittance of the microphone must be known in absolute terms at one low or medium-low frequency. This admittance can be found with the same methods used hitherto for the lumped parameter model
- At low and medium frequencies the new representation is an improvement as compared to the lumped parameter model traditionally used in reciprocity calibration of microphone pressure sensitivity. At high frequencies the representation is an improvement for LS1 microphones and for LS2 microphones the new representation and the lumped parameter model seem to be equally adequate
- The difference between calibration results calculated with the lumped parameter method and the proposed representation is of the same order of magnitude as the uncertainty of measurement that can be obtained as of today. There is therefore a need for validation of the representation and the differences should be accounted for in uncertainty budgets for reciprocity calibrations
- The proposed admittance representation can be used to obtain improved results in a simple way with the pairs of a long and a short coupler widely used in calibration laboratories, provided the compliance of the microphone diaphragm (the equivalent volume) is available with sufficient accuracy.

Possible improvements of the determination the compliance are under consideration

Acknowledgements

The authors gratefully acknowledge the work by and the many discussions with Salvador Barrera-Figueroa and the late Knud Rasmussen, Danish Fundamental Metrology, that has led to the considerations behind this paper. The authors also gratefully acknowledge Brüel & Kjær Sound & Vibration Measurement A/S for recognizing the importance of the work with primary calibration.

References

[1] IEC 61094-2:2009, Measurement microphones – Part 2: Primary method for pressure calibration of laboratory standard microphones by the reciprocity technique, IEC (2009)

[2] Erling Sandermann Olsen, "Heat conduction correction in reciprocity calibration of laboratory standard microphones", presented at INTER-NOISE 2012, New York, (1994).

[3] IEC 61094-1:2000, Measurement microphones – Part 1: Specifications for laboratory standard microphones, IEC (2000)

[4] COMSOL Multiphysics version 4.3a, Finite element modeling software by COMSOL (2013)

[5] Erling Sandermann Olsen and Mads Herring Jensen, "Virtual prototyping of condenser microphones using the finite element method for detailed electric, mechanic, and acoustic characterization", presented at ICA 2013, Montreal, (2013)

[6] Knud Rasmussen, "Determination of microphone parameters by datafitting", DPLA Calibration Workshop, Brüel & Kjær (2003)

[7] Brüel & Kjær, "Product Data Reciprocity Calibration System Type 9699, Reciprocity Calibration Apparatus Type 5998" (1997)

[8] Brüel & Kjær, "Product Data WZ-0078 and WZ-0079, Plane Wave Coupler Sets for Microphone Reciprocity Calibration"

Previously issued numbers of Brüel & Kjær Technical Review

(Continued from cover page 2)

Special technical literature

Brüel & Kjær publishes a variety of technical literature that can be obtained from your local Brüel & Kjær representative.

The following literature is presently available:

- Catalogues
- Product Data Sheets

Furthermore, back copies of the Technical Review can be supplied as listed above. Older issues may be obtained provided they are still in stock.

Front cover: Offshore wind turbines near the coast of Denmark

Each Brüel & Kjær Technical Review contains a collection of technical, scientific articles that describe theory, measurement techniques and instrumentation, which are specifically aimed at acousticians and vibration engineers.

See more on **bksv.com/library**, Technical Reviews

BV 0066 – 11 2014-11

Brüel & Kjær Sound & Vibration Measurement A/S
DK-2850 Nærum · Denmark · Tel: +45 77 41 20 00 · Fax: +45 45 80 14 05
www.bksv.com · info@bksv.com
Local representatives and service organisations worldwide